H_2: entanglement, probability density function, confined Kratzer oscillator, universal potential and (Mexican hat- or bell-type) potential energy curves

G. Van Hooydonk, Ghent University, Faculty of Sciences, Ghent, Belgium

Abstract. *We review harmonic oscillator theory for closed, stable quantum systems. The H_2 potential energy curve (PEC) of Mexican hat-type, calculated with a confined Kratzer oscillator, is better than the Rydberg-Klein-Rees (RKR) H_2 PEC. Compared with QM, the theory of chemical bonding is simplified, since a confined Kratzer oscillator gives the long sought for universal function, once called the Holy Grail of Molecular Spectroscopy. This is validated with HF, I_2, N_2 and O_2 PECs. We quantify the entanglement of spatially separated H_2 quantum states, which gives a braid view. The equal probability for H_2, originating either from H_A+H_B or H_B+H_A, is quantified with a Gauss probability density function. At the Bohr scale, confined harmonic oscillators behave properly at all extremes of bound two-nucleon quantum systems and are likely to be useful also at the nuclear scale.*

Introduction

Since the harmonic oscillator (HO) is essential for physics [1] and chemistry [2], understanding H_2, the simplest, prototypical oscillator in nature, is important. While H is prototypical for atoms with simple Bohr theory, H_2 is prototypical for bonds but no simple oscillatory bond theory exists [2]. Inverting levels with RKR (Rydberg-Klein-Rees [3]) or IPA (inverted perturbation approximation [4]) gives the H_2 potential energy curve (PEC) [5]. We revisit the H_2 oscillator and bring in the long sought for universal potential energy function (UPEF) [6-10], once called the *Holy Grail of Molecular Spectroscopy* [11]. A new approach is needed, since QM fails on an analytical potential energy function (PEF), even for H_2 [5,11].

Vibrational H_2 levels U_v, nearly parabolic in quantum number v, transform in H_2 PEC U_r, nearly parabolic in r but with different curvatures and extremes. We merge all curvatures and extremes in a single PEF, using the classical ionic Kratzer-Coulomb potential [12] for H_2 [13]. The Kratzer H_2 PEC is more precise than the RKR PEC, if 2nd order Kratzer function is upgraded to 4th order. This gives a Mexican-hat type PEC for H_2 and a parameter free UPEF, although a low parameter UPEF may not even exist [6-10,11,14]. Our RKR-based solution bears on entanglement of spatially separated H_2 quantum states. This gives a braid effect, important for EPR-paradox and Bell inequalities [15] and quantum information theory [16], and simplifies the theory of the chemical bond [17]. This also provides with a link between the physics in a Kratzer model and probabilities (entropy). We show that the Mexican hat-type UPEC for H_2, HF, I_2, N_2 and O_2 is complementary with their bell curve for normal Gauss probability density distributions.

The outline is as follows. In Section II, we review problems. Section III is on a confined Kratzer harmonic oscillator, which generates a Mexican-hat type PEC for H_2. Results are in Section IV. Section V gives 6 applications: entanglement, universal function, scaling, Gauss probability density function, theory of the chemical bond and QM H_2 PEC. Section VII concludes.

Known problems with variables/curvatures and shortcomings of parabolic HO

(a) Choice of variables and asymptotes for PECs

Standard PECs use inter-atomic separation r and the scaled Hooke-Dunham variable [18]

$$\delta_D=r/r_0,\ \delta_D-1=r/r_0-1 \quad (1)$$

However, it is well known that the widely used molecular Dunham function[1,2] $U_{r,D}$, starting off as

$$U_{r,D}=U_0(1-r/r_0)^2+\ldots=D_e(1-r/r_0)^2+\ldots=\tfrac{1}{2}k_e r^2{}_0(1-r/r_0)^2+\ldots \quad (2)$$

is wrong. It can never converge at large r [19] and needs higher order terms to secure moderate convergence [17], though it uses the correct well depth, covalent bond energy D_e for $H+H\rightarrow H_2$. The less used inversely scaled Coulomb-Kratzer variable [12]

$$\delta_K=r_0/r,\ \delta_K-1=r_0/r-1 \quad (3)$$

gives an ionic molecular Coulomb-Kratzer oscillator potential

$$U_{r,K}=U_0(1-r_0/r)^2=D_{ion}(1-r_0/r)^2 \quad (4)$$

This does without higher order terms, is superior in many respects to (2) and always converges to ionic bond energy D_{ion} for $H^+ + H^-\rightarrow H_2$, larger than D_e. A choice for D_e or D_{ion} is a choice for (1) or (3). All results of Kratzer model (4) for H_2 are given in Appendix A. We remind (4) is also useful for nuclear physics [20].

(b) RKR turning points as a generic basis of the entanglement of quantum states

In a PEC, linear turning points $r_\pm$ are at either side of r_0; inverse turning points $1/r_\pm$ are at either side of $1/r_0$. To extract these from energies U_v, RKR uses f and g, both complex Klein functions of levels ΔU_v, respectively $F(\Delta U_v)$ and $G(\Delta U_v)$ [3], defined as

$$2f=r_R-r_L=F(\Delta U_v);\ 2g=1/r_L-1/r_R=G(\Delta U_v);\ f/g=r_R r_L \text{ and } g/f=1/(r_R r_L) \quad (5)$$

This connection between ΔU_v and Δr leads to continuous PEC U_r. However, (5) allows linear as well as inverse turning points at the same time

$$r_\pm=\sqrt{(f/g+f^2)}\pm f=\tfrac{1}{2}(r_+ + r_-)\pm\tfrac{1}{2}(r_+ - r_-)=\tfrac{1}{2}(r_+ + r_-)(1\pm I) \quad (6)$$

$$1/r_\pm=\sqrt{(g/f+g^2)}\pm g=\tfrac{1}{2}(1/r_+ + 1/r_-)\pm\tfrac{1}{2}(1/r_+ - 1/r_-)=\tfrac{1}{2}(1/r_+ + 1/r_-)(1\pm I) \quad (7)$$

The reduced difference I between turning points is

$$I=(r_+ - r_-)/(r_+ + r_-)=(1/r_- - 1/r_+)/(1/r_+ - 1/r_-)=(A-B)/(A+B) \quad (8)$$

With (6)-(7), RKR has no preference for $r_\pm/r_0$ in (2) or for $r_0/r_\pm$ in (4). This makes it difficult to understand why inverse Kratzer turning points $r_0/r_\pm$ are hardly used, see (a). Coupling I, $r_\pm$ and r_0

$$r_\pm=r_0(1\pm I)^{\pm 1} \quad (9)$$

conforms to the difference between (1) and (3). As I is independent of a scale factor for $r_\pm$, we

[1] Eqn. (2) is part of the full Dunham potential, an expansion in d_D (1), i.e. $U=a_0 d_D{}^2(1+a_1 d_D+a_2 d_D{}^2+\ldots)$, with Dunham coefficients a_n. In a polynomial in $(v+\tfrac{1}{2})$ and J(J+1), i.e. $U=\Sigma\, Y_{nm}(v+\tfrac{1}{2})^n[J(J+1)]^m$, Y_{nm} are also Dunham coefficients but the complex relation between a_n and Y_{nm} is, however, not relevant here.

[2] A Taylor expansion brings in the very same lead term for the Morse potential [21].

use (9) and do not consider generalization $r_{\pm}=r_0(1\pm I)^{\pm n}$, where n is different from 1.

Table 1. H_2 data in [5] and this work (r in Å, U_v in eV)(r_0=0,74173, D_e=4,7476, D_{ion}=9,7069 [5])

r [5]	U_v [5]	r reversed[a]	r/r_0-1	r_0/r-1	I	$r=r_0/(1\pm I)$	v+½[b]
0,4109	4,729	3,2835	-0,446025	0,805135	0,777555	0,41723	14,5
[0,4158][b]	4,522	2,3748	-0,43945	0,783965	0,702014	0,43579	12,5
0,4319	3,88	1,8524	-0,417713	0,717365	0,621854	0,45733	9,5
0,4597	2,935	1,5148	-0,380233	0,613509	0,534363	0,48341	6,5
0,5088	1,73	1,2186	-0,314036	0,457803	0,410907	0,52571	3,5
0,6337	0,269	0,8833	-0,145646	0,170475	0,164535	0,63693	0,5
0,74173		0,74173	0,000000	0,000000	0,000000	0,74173	
0,8833	0,269	0,6337	0,190865	-0,160274	-0,164535	0,88781	0,5
1,2186	1,73	0,5088	0,642916	-0,391326	-0,410907	1,25910	3,5
1,5148	2,935	0,4597	1,042253	-0,510345	-0,534363	1,592937	6„5
1,8524	3,88	0,4319	1,497405	-0,599584	-0,621854	1,96149	9,5
2,3748	4,522	[0,4158][b]	2,201704	-0,687666	-0,702014	2,48914	12,5
3,2835	4,729	0,4109	3,426813	-0,774104	-0,777555	3,33444	14,5
[4,23[c]	4,745		4,702884	-0,824650			?]
[6,35[c]	4,747		7,561067	-0,883192			?]

[a] r in reversed order absent in [5], since entanglement was not considered
[b] not given in [5] but computed here to have a complete set
[c] these last two energy values in [5] are not observed values, see also Table B1

By definition, (6)-(7) expose state entanglement. They create two sets of algebraically connected turning points for U_r: one in increasing order (from small to large), the other in reverse order (from large to small), as shown in Table 1. Using both sets gives an experimentally validated knot or braid view on H_2, discussed further below.

(c) Parabolic behavior of levels U_v in function of v+½

H_2 levels are parabolic in v+½, if zero point energy ZPE is included. Integer v applies for levels without ZPE [13](see Appendix B). The latter obey the inverse Kratzer variable (5), rewritten as

$$r_0/r_+-r_0/r_-=1/(1-½Av\omega/D_{ion})-1/(1+½Av\omega/D_{ion})=Av(\omega/D_{ion})/[1-¼(Av\omega/D_{ion})^2] \quad (10)$$

where ω is the harmonic frequency, constant A is close to 1 (A=0,838 [13]). Ratio ω/D_{ion}= 4410/78844,9=17,87 provides with $v_0=v_{max}$ (see [13] and appendix A). Since $Av(\omega/D_{ion})/[1-¼(Av\omega/D_{ion})^2]\approx Av/v_0+\ldots$, a plot of U_v versus v/v_0 gives correct first order curvatures, since U_v

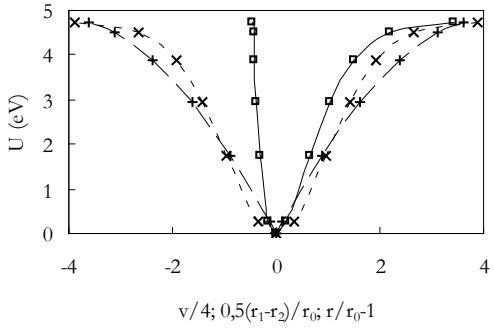

Fig. 1 U_v (eV) versus (v+½)/4 (long dashes +); r/r_0-1 (full □) and ½(r_+-r_-)/r_0 (short dashes x)

$\approx[1-(1-v/v_0)^2]+\ldots=2(v/v_0)-(v/v_0)^2+\ldots=2x-x^2+\ldots$as shown in the right part of Fig. 1 (long dashes

+). This right part can be extended to the left side as in Fig. 1 but on doing so, fitting the complete set in v/v_0 becomes problematic. With these 3 problems in mind, we turn to levels and PECs for H_2. Fig. 1 shows U_v, plotted versus $\pm(v+½)/4$, using scale factor 4 to make this parabola commensurate with the RKR PECs in $r_\pm/r_0$-1and $½(r_+-r_-)/r_0$). U_v and U_{diff} approach the asymptote at either side. U_v crosses the origin, which is approached by U_{diff}. Although continuous r/r_0-1 PEC approaches the origin also, only its attractive (right) branch approaches the limit at large r, due to a curvature switch. Its repulsive (left) branch seems to cross this at small r and no switch in curvature shows. PECs in r/r_0 in Fig. 1 cannot be fitted reasonably but PECs in r_0/r in Fig. 2 can. This shows in Fig. 2 with H_2 PECs based on inverse turning points. The U_v plot for $\pm v/v_0$ is now compared with continuous $r_0/r_\pm$-1 and difference $½(r_0/r_+-r_0/r_-)$ PECs. A scale factor for v/v_0, between -1 and +1, is not needed. Curvatures for PECs are different from those in Fig. 1. PECs are similar and almost left-right symmetrical. The difference PEC obeys quite accurately 2nd order (parabolic) and 4th order (quartic) fits (see below).

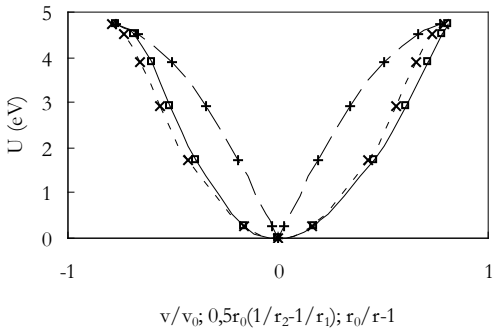

Fig. 2 U_v (eV) plotted versus v/v_0 (long dashes +); r_0/r-1 (full □) and $½(1/r_+-1/r_-)r_0$ (short dashes x)

The similar curvatures for PECs are opposite to those for U_v. Both PECs approach origin as well as limit $U_0=D_e$. These 3 problems (a-c) have important implications.

(d) Shortcomings of parabolic HO behavior: the confined or closed quartic harmonic oscillator (CHO)

First and as stated above, PECs in r/r_0 cannot be fitted, whereas those in r_0/r can [13,17]. Second, the shape of the H_2 PEC depends on the variable: Dunham r/r_0 (1) gives asymmetric (Fig. 1), Kratzer r_0/r (3) symmetric PECs (Fig. 2). Since both are compatible with RKR (6)-(7), r_0/r seems superior a variable as to bond symmetry than r/r_0, as argued in [17].

Third, the HO parabola with its single extreme, approached by either branch, is deceptive: its infinite branches always cross natural limit U_0. With parabolic HO behavior, the H_2 dissociation limit would always be crossed or, a HO is always wrong for prototypical natural oscillator H_2. While HOs have open branches, natural CHOs have finite branches, confined to $U_0=D_e$. This means that in either branch, a switch of curvatures must occur.

Confined harmonic oscillator (CHO) for H_2: from Kratzer parabola to Kratzer quartic

(a) Trivial Kratzer HO: turning points in a parabolic PEC

Without knowing D_e, an ionic Kratzer model with difference d between turning points gives

$$U_v=D_{ion}d^2=¼D_{ion}(r_0/r_- - r_0/r_+)^2 \quad (11)$$

with trivial solutions

$$d=\pm\sqrt{(U_v/D_{ion})} \quad (12)$$

Although this parabolic Kratzer HO reproduces levels exactly, its turning points must be tested with those from RKR using (9) with d≈I (D_{ion}=9,707 eV for r_0=0,74173).

Fig. 3 shows the U_v(d) plot and RKR PECs in $d_i'=½r_0(1/r_1-1/r_2)$ and $d_i''=r_0/r_\pm-1$. Despite the simplicity of (11), RKR PECs are close to this ionic Kratzer PEC. The parabolic Kratzer fit in d

$$U_v= 9,3d^2\approx D_{ion}d^2 \text{ eV} \quad (13)$$

has goodness of fit $R^2\equiv1$. Ionic Kratzer turning points d are further discussed in Table 3 below.

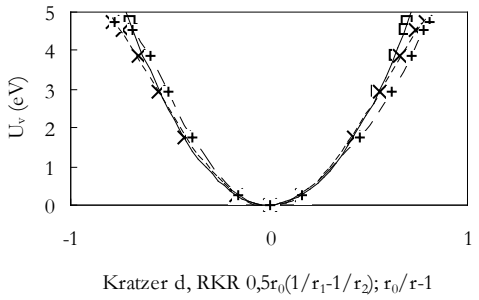

Fig. 3 U_v versus d (full), d_i' (short dashes) and di" (long dashes)

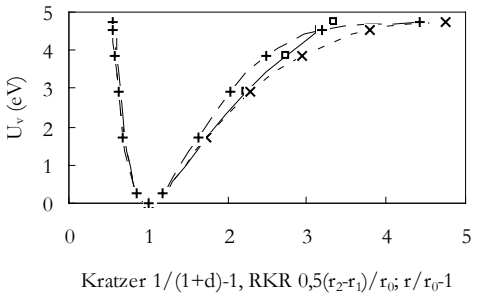

Fig. 4 U_v versus $1/(1\pm d)-1$; d' (short dashes) and d" (long dashes)

In a trivial Kratzer approach, D_e is not required, since any non-zero asymptote U_0=D reproduces levels exactly but turning points must be meaningful. With this criterion, ionic bond energy D_{ion} leads to the best results (see below). Although D_{ion} is much larger than covalent well depth D_e, we find that, unlike its depth, the width of the well is governed, for the larger part (see Fig. 4), by ionic Coulomb-Kratzer limit $D_{ion}=½e^2/r_0$, not by D_e (see Appendix A and [13]).

A quartic fit for the RKR difference PEC using turning points d' [13]

$$U_v=-5,3759d'^4 + 11,089d'^2 \text{ eV} \quad (14)$$

has a much smaller goodness of fit R^2 = 0,9982 (see Table 3 below).

Using (9), the trivial Kratzer approximation is easily extended to variable r/r_0. Fig. 4 shows PECs for $1/(1\pm d)-1$ and those for RKR $½(r_1-r_2)/r_0$ and $r_\pm/r_0-1$. Even with r/r_0, a Kratzer potential accounts nicely for 95 % of the complete PEC, which is surprising. While errors for levels are zero (exact result), the difference with RKR turning points is only 4 % (see Table 3). Since trivial

Kratzer HO (13), like all other parabolic HOs, is open and does not behave properly at limit D_e, also this plausible Kratzer HO must, mathematically, be upgraded at least to order 4 (CHO).

(b) From parabola (HO) to quartic (CHO) and Mexican hat potential energy curve

Observed U_v shows a parabolic dependence on v/v_0, see at (10) and Fig. 1-2, with D_e as natural limit (the theory [13] is in (c) below). For any non-zero D, U_0=D and $x=v/v_0$ give a parabola and trivial but always exact solutions, respectively obeying

$$U_v=U_0(2x-x^2)=D(2x-x^2);\ U_v/D=y=2x-x^2 \text{ and } 1-y=(1-x)^2 \quad (15)$$

$$x_{\pm}=1\pm\sqrt{(1-U_v/D)}=1\pm\sqrt{(1-y)}=1\pm(1-x) \quad (16)$$

As in (a), (15) returns all levels exactly by definition but parabolic turning points (16) must make sense. An alternative parabola for (15) is obtained with turning points $x'=\pm\sqrt{(2x-x^2)}$ or $y=x'^2$. Again this is still exact for levels but can be meaningless for points x', pending the value of D.

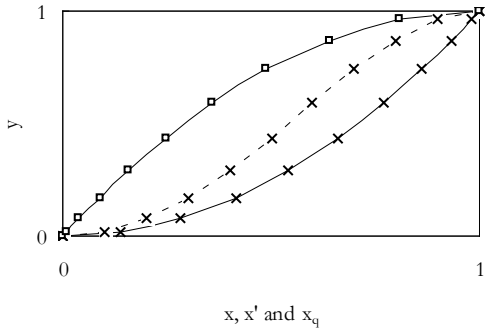

Fig. 5 Plot of y versus x (full □), x' (full x) and x_q (dashes x)

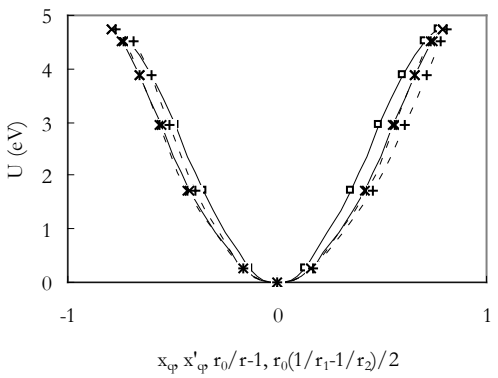

Fig. 6 Kratzer quartic H_2 PECs in x_q (full □), x'_q (full x), $r_0/r-1$ (dashes +), $½(r_0/r_1-r_0/r_2)$ (dashes *)

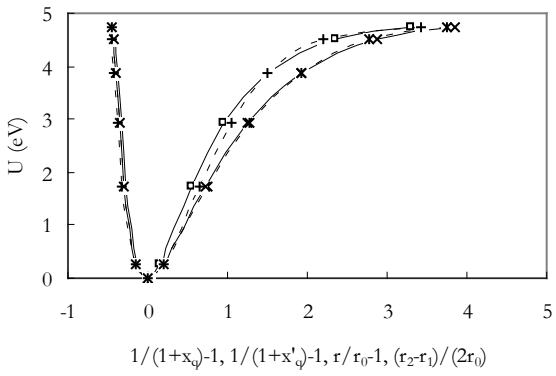

Fig. 7 Dunham quartic H_2 PECs in $1/(1+x_q)-1$ (full □), $1/(1+x'q)-1$ (full x), r/r_0-1 (dashes +), $½(r_2/r_0-r_1/r_0)$ (dashes *)

Mathematically, the simplest way to get a confined HO or CHO is to go over to the square root of x or $\sqrt{x}$, the generic variable x_q to obtain a Kratzer quartic. With (16), quartic turning points

$$x_q=\pm\sqrt{[1-\sqrt{(1-U_v/D)}]}=\pm\sqrt{x} \quad (17)$$

will also reproduce exactly the very same H_2 levels U_v of (15), following the Kratzer-type quartic

$$U_v=U_0(2x-x^2)\equiv U_0[2(\sqrt{x})^2-(\sqrt{x})^4]=U_0(2x_q^{\,2}-x_q^{\,4})=U_r \quad (18)$$

Due to (10), x_q is naturally connected with slightly smaller variable x'_q, derived from

$$x_q=x'_q/(1-x'^{\,2}_q/4) \text{ or } x'_q=(-2/x_q)[1\pm\sqrt{(1+x_q^{\,2})}] \quad (19)$$

The mathematical advantage of quartic (18) is that it creates critical points at either side of the minimum, with accompanying curvature switches (see Fig. 5-6). Given the similarity of U_v and PEC U_r behavior (15)-(18), it is only natural to allow for some scale factor A for x_q to switch from U_v to U_r. Kratzer type PECs for A=0,7925≈0,8 in Fig. 6, can be compared with those in Fig. 3; Dunham-type PECs in Fig. 7 with those in Fig. 4. From Fig. 7, it appears that Ax_q, is related to $r_0/r-1$ in RKR; x'_q to $½r_0(1/r_1-1/r_2)$. Obviously, all 3 Kratzer PECs are of Mexican-hat type, but only the PEC in $0,8x_q$ (X) is exact. Details are in Table 3. The connection of x'_q in (19) with the RKR difference is nearly one by one (see Fig. 7).

(c) Theoretical treatment using vibrational quantum numbers v+½ [13]

To find a PEC using Kratzer connection (10) between v/v_0 and ΔU_v, the values of v+½, not given in [5], are needed. Following the analysis in [13], v+½ is included in Table 1.

A useful application of (15), which is also a stringent accuracy test of a Kratzer bond theory [13], is provided by the transition to complementary variable x'=1-x. This transition obeys

$$U_v=U_0(2x-x^2)=U_0[2(1-x')-(1-x')^2]=U_0(1-x'^2) \quad (20)$$

which implies that a plot of U_v versus x' gives U_0 as *maximum* intercept, when the coefficient for linear x' has vanished since 2x'-2x'=0. With this consistency procedure, we found [13] that

$$x'=a[1/(1-0,022426(v+½)-1/(1+0,022426(v+½)] \quad (21)$$

provides immediately with D_e. The result of (21) with the less precise level data in [5] for (20) is 38321,58 cm^{-1} for the intercept and 38259,36 cm^{-1} for the slope. Their average 38290,47 cm^{-1} is close to 4,7476 eV=38292 cm^{-1} in [5]. For the theoretical PEC U_r based on (20)-(21), variable √x' must be used, due to (17).

More precise results would be obtained if more precise observed levels [22] were used as in [13]. We pertain to data in [5], see Table 1, to keep this analysis of the RKR procedure transparent.

Classical proof for CHOs and quartic PECs instead of HOs

A classical justification for CHOs is compatible with Klein RKR equations (6)-(8). Using $r_A=r_+$ and $r_B=r_-$ for $r_\pm$ in (9), all possible analytical forms for variables and PECs, centered at the origin, are in Table 2. With both Dunham and Kratzer variables (1) and (3), parabolic HOs and PECs to order 2 are easily completed with 4th order CHOs or PECs, pending the algebraic choices for (9). Since only one set of observed differences ΔU_v is available, standard solution $\Delta U_v=D_e=I$ gives a difference PEC in 2nd order I^2 (see lines for f and g in Table X). However, interpreting the same

difference with continuous PECs in $(r_{AB}/r_0\text{-}1)^2$ or $(r_0/r_{AB}\text{-}1)^2$, where $r_{AB}=½(r_A+r_B)$, gives $\Delta U_v=I^2$ and PECs in 4th order I^4. This classical proof justifies the CHOs needed.

Even the zero PEC-cases are of interest, since the straight line prediction can immediately reveal if r_A and r_B obey (9).

Table 2. Inventory of all variables and PECs through the origin possible with algebraic (9).

Variable	Option (a) $r_\pm=r_0(1\pm I)$	PEC[a]	Option (b) $r_\pm=r_0/(1\pm I)$	PEC[a]
$s=r_{AB}/r_0=½(r_A+r_B)/r_0$	1	$(1\text{-}s)^2=0$	$s=1/(1\text{-}I^2)$	**$I^4/(1\text{-}I^2)^2$**
$(f/g)/r^2_0=r_Ar_B/r^2_0$	$1\text{-}I^2$		$(f/g)/r^2_0=1/(1\text{-}I^2)$	
$f=½(r_A\text{-}r_B)/r_0$	I	$f^2=I^2$	$f=I/(1\text{-}I^2)$	$I^2/(1\text{-}I^2)^2$
$s'=½r_0(1/r_A+1/r_B)$	$1/(1\text{-}I^2)$	**$I^4/(1\text{-}I^2)^2$**	$s'=1$	$(1\text{-}s'^2)=0$
$g=½r_0(1/r_B\text{-}1/r_A)$	$I/(1\text{-}I^2)$	$g^2=I^2/(1\text{-}I^2)^2$	$g=I$	I^2
$(g/f)r^2_0=r^2_0/(r_Ar_B)$	$1/(1\text{-}I^2)$		$(g/f)r^2_0=1\text{-}I^2$	
$s''=r_0/r_{AB}=2r_0/(r_A+r_B)$	1	$(1\text{-}s'')^2=0$	$s''=(1\text{-}I^2)$	**I^4**

[a] PECs, expected classically to be of 4th order, are given in bold

With Table 2, the internal consistency of RKR turning points in [5] is easily verified. Scale invariant I cannot only be calculated from (8) but also from sum and product of turning points. Option (b) gives $I_s=\pm\sqrt{(1\text{-}r_0/r_{AB})}$ in the bottom row and $I_p=\pm\sqrt{[1\text{-}r^2_0/(r_Ar_B)]}$ in row g. This implies that I in (8) be denoted by I_0. If state entanglement were to hold exactly as in (9), $I_0=I_s=I_p$.

Since all I-values are easily calculated from RKR turning points in Table 1, a comparison with the trivial spectroscopic I-value, i.e. $0{,}8x_q$ (17) or its theoretical value from (21) is in order. The % differences generated by I_0, I_s, I_p, $r_0/r\text{-}1$ and $½_0r_0(1/r_A\text{-}1/r_B)$ are all given in Table 3 below.

With this criterion, I_s with 3,4 % difference is the better RKR choice for $0{,}8x_q$ (see also below).

With the relatively large errors for U_v in Table 3, generated by I_0, I_s, I_p, $r_0/r\text{-}1$ and $½_0r_0(1/r_A\text{-}1/r_B)$, it is difficult to validate H_2 RKR turning points in [5].

Table 2 explains why parabolic oscillator (15) and quartic (18) are completely equivalent for levels but return different turning points (see Fig. 5): parabolic turning points are $\pm x$ (16), quartic turning points are (18) $\pm\sqrt{x}$. This is the sole reason why the HO for natural, prototypical oscillator H_2 is a quartic CHO, giving a Mexican hat type PEC, with finite branches, approaching limit $U_0=D_e$ at either side of the minimum without ever crossing it.

Mexican hat curves, generated by a CHO, are, however, complementary to bell or Gauss curves. This brings in a probabilistic interpretation for H_2, which will be discussed further below.

Results and interpretation

Table 3 compares all results with emphasis on internal consistency, analytical simplicity and accuracy. For transparency, we use U_v in [5] instead of those in [22]. Data are in Tables 1 and B1.

PEC 1: the trivial Kratzer method (13) for $D_{ion}=9{,}3$ eV, gives 4,2 % difference for 10 out of 12

RKR turning points, excluding the 2 outermost. Differences ΔI with RKR $½(r_1-r_2)/r_0$ are 4,2 % for 12 and only 2,32 % for 10 RKR points. This is amazing as levels are reproduced exactly. It explains why a trivial Kratzer approach accounts nicely for >90 % of the H_2 PEC, see Fig. 3-4.

Table 3. Accuracy and simplicity of Kratzer HO and 2 CHOs for the H_2 PEC, compared with RKR [5]

Nr Type	variable x	U_r (eV)	ΔU cm^{-1}	ΔU%	Δr(ΔI)%
PECs from this work					
1 Kratzer[a]	$x=\pm\sqrt{(U_v/D_{ion})}$ (13)	$9{,}30000x^2$	0	0	4,2[b](2,3)
2 CHO[a,c]	$0{,}8x_q$ in (18)	$-11{,}590820x^4+14{,}836250x^2$	0	0	4,19(3,2)
3 CHO_{theo}	$0{,}8\sqrt{x}$' in (21)	$-11{,}530711x^4+14{,}803444x^2$	5,4	0,04	4,24(3,2)
PECs from turning points $r_\pm$ in [5] from their difference and from I_0,I_p and I_s					
4 CHO[d]	$r_0/r_\pm-1$	$-5{,}75796x^4+1{,}30523x^3+11{,}23558x^2-1{,}101037x$	916,8	12,52	
5 CHO[d] (8)	$I_0=(r_A-r_B)/(r_A+r_B)$	$-7{,}606082x^4+12{,}628366x^2$	953,0	7,80	
6 CHO[d]	$½r_0(1/r_A-1/r_B)$	$-5{,}375916x^4+11{,}089020x^2$	573,5	3,99	
7 CHO[d]	$I_p=\sqrt{(1-r^2{}_0/r_Ar_B)}$	$-15{,}608616x^4+17{,}208229x^2$	160,9	1,77	
8 CHO[d]	$I_s=\sqrt{(1-r_0/r_{AB})}$	$-11{,}302032x^4+14{,}775512x^2$	617,5	5,64	
Morse PEC: (a) U_v from RKR turning points; (b) Morse turning points from U_v					
9a Morse	U_v from RKR r	$D_e\{1-\exp[-2{,}084(r-r_0)]\}^2$		463,9	3,68
9b Morse	r from U_v	$D_e\{1-\exp[-2{,}084(r-r_0)]\}^2$		0	0 3,3(-)

[a] generic methods for respectively the trivial Kratzer ionic HO model using U_v/D_{ion} and the trivial CHO using U_v/D_e
[b] only for this HO, the % differences applies for all turning points, except the 2 outer extremes, see Fig. X
c coefficient for x^2 is $2D_e/0{,}8^2=3{,}215D_e=14{,}83625$; for x4 this is $De/0{,}8^4=2{,}4414D_e=11{,}59082$
[d] all variables calculated with the turning points in [5], collected in Table 1

PEC 2: This second trivial method uses solely levels U_v and D_e as input for turning points (18). Comparing this result with RKR using $0{,}8x_q$ (17) gives a difference of 4,19% for 12 turning points, including the 2 outer ones and 3,2 % for I_s. As for PEC 1, all levels are returned exactly. PECs in $\pm Ax_q$ are of Mexican hat-type (Fig. 6), those in $1/(1\pm Ax_q)-1$ are not (Fig. 7).

PEC 3: The theoretical approach has the advantage over PEC 2 that D_e is also directly available from U_v using (20) [13]. Moreover, PEC 3 is almost indistinguishable from PEC 2. Differences for levels of 5 cm^{-1} (0,04 %) are in line with [13]. Improving its precision is possible [23].

Despite their analytical simplicity, PECs 1-3 of this work are of spectroscopic accuracy as they reproduce levels exactly at the expense of small differences (≤4%) with RKR turning points. Since turning points are not observed but are expectation values, pending the models (RKR, IPA), PECs 2-3 are plausible for H_2. PEC 2 is trivial but exact. Fully theoretical PEC 3 is less exact but more complete on the physical implications. PECs 2-3 are of Mexican hat type and derive from a CHO, not from a HO, following the proof above.

PECs 4-8: If RKR were really reliable, it is normal to expect that fitting U_v versus its own turning points should be reasonably accurate. Fits to order 4 should therefore give small, if not zero differences for U_v. Surprisingly, RKR PECs 4-8 do not give small errors at all (see Table 3). Errors between 161 and 953 cm^{-1} (0,02 and 0,12 eV) in % are much larger than t% errors for r(I)

with the PECs 1-3. This shows that the quality of PECs 2-3 is better than any RKR PEC.
PEC 8: For comparison and without further comments, we give accuracy details for the well-known Morse potential [21], (unjustly) much more used than Kratzer's [12].
Although details are barely visible in graphs, we nevertheless give 2 more figures. Fig. 8 shows the more symmetric behavior of PECs 2-3 in this work and RKR PECs 5, 7 and 8 using inverse (Kratzer) turning points r_0/r (3). Fig. 9 shows the rather asymmetric, conventional PECs 2-3 in this work, RKR PECs 4 and 8 and Morse PEC 9 using linear (Dunham) turning points r/r_0 (1).

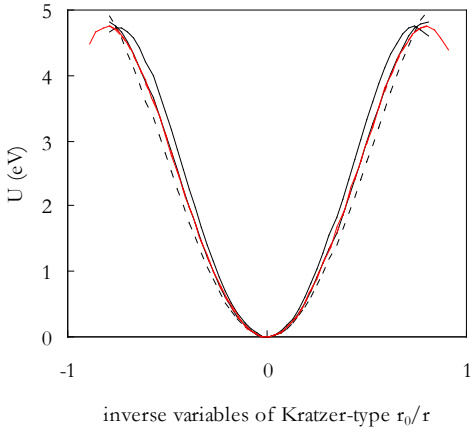

Fig. 8 PEC 2 (red full), 3 (red dashes), 5 (black mixed dashes) 7 (black dashes) and 8 (black full)

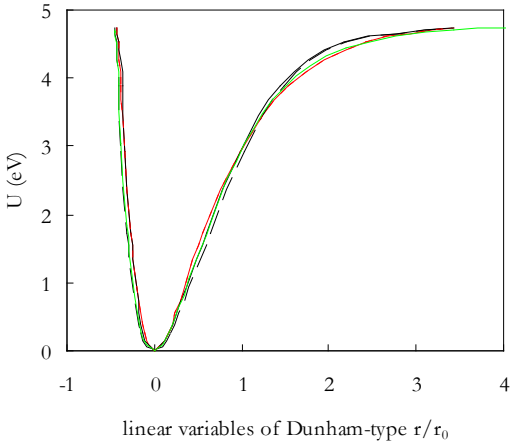

Fig 9 PEC 2 (red full), 3 (red dashes), 4 (black long dashes), 8 (black full) and Morse 9 (green)

In Fig. 8, PEC 8 nearly coincides with the single curve for both 2 and 3, as expected from the analytical resemblances in Table 3. We also extrapolated the fit for exact PEC 2 to verify that this is indeed a Mexican hat-type curve, showing that no branch crosses limit D_e. However, H_2 states beyond the external inflection points are imaginary and cannot be observed according to this theory. In contrast, Fig. 9 suggests that the left branch of all PECs in r/r_0 would cross this limit when extrapolated to lower r. This wrong information on prototypical diatomic bond H_2 is probably the major shortcoming of PECs in Dunham variable r/r_0 (1) and of the Morse PEC. Despite this, PECs in Fig. 9 appear in many textbooks on molecular spectroscopy, whereas equally valid PECs in Fig. 8 with inverse turning points are hardly used.
The rather disappointing accuracy tests for PECs 4-8 are not really surprising, reminding that RKR evolved from a graphical (Rydberg [3a]) to a semi-empirical WKB approximation (Klein-Rees [3b,c]) and that a number of complicated steps is needed to link ΔU_v. with Δr (see for instance [24]). Since we succeeded in using only a single and analytically simple step to establish this link between ΔU_v and Δr, more applications emerge.

Applications

(a) Entanglement of H_2 quantum states

Understanding entanglement of spatially separated quantum states is important for the EPR-paradox and Bell inequalities [15], quantum information theory and computing [16], topological entropy, non-locality…. We illustrate entanglement of spatially separated H_2-states, essentially given away by RKR as shown in Section II. We interpret observed H_2 frequency gaps ΔU_v as radial differences (separations) Δr on field axis r.

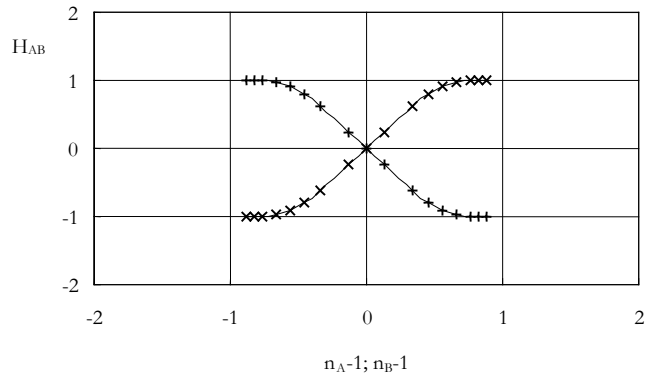

Fig. 10 Plot of H_{AB} versus n_A-1 for H_A-states (full x) and n_B-1 for H_B-states (dashes +)

Absolute differences are $|r_A-r_0|$ for atom H_A and $|r_B-r_0|$ for atom H_B if r_0 is the equilibrium bond length. With H_A far away at $r_A=r_0/(1-I)>>r_0$ (I=0,99 gives $r_A=100r_0$), its dimensionless number is

$$n_A=r_0/r_A=1-I \text{ or } n_A-1=-I \quad (22)$$

Classical RKR physics (6)-(8) automatically fixes r_B for partner H_B at $r_B=r_0/(1+I)$ or at number

$$n_B=r_0/r_B=1+I \text{ or } n_B-1=I \quad (23)$$

(I=0,99 gives $0{,}502r_0$ with lower limit $½r_0$=0,37086 Å at I=1).

Next, the square root of reduced U_v/D_e gives similar numbers for the spectrum of bond H_2, i.e.

$$H_{\pm}=H_{AB}=\pm\sqrt{(U_v/D_e)} \quad (24)$$

A combination of all these numbers for H_2 leads to a braid plot of H_{AB} versus n_A-1and n_B-1 as shown in Fig. 10. The advantage of a braid view over that with PECs/CHOs, as above, is that it nicely illustrates why the choice for H_A and H_B is arbitrary. Interchanging suffixes, i.e. allowing for H_B and H_A also, is allowed and even essential. This is also a cornerstone of QM theory of the chemical bond (LCAO, VB and MO methods [2]). Entanglement of H-states at any separation from the center, large or small, is clearly exposed in the braid view in Fig. 10 and by (22)-(23). Conceptually, entanglement of H_2 states is secured by the fact that the very same frequency gaps ΔU_v are used to fix radial separations Δr at either side of the minimum. Braid views are important for theory, following [25] in a comment on recent experiments on entanglement [26].

(b) Universal molecular potential energy function (UPEF)

The importance of a universal function is evident when looking at the 5 PECs in Fig. 11 for H_2, HF, I_2, N_2 and O_2 in [5]. Scaling U_v and r or 1/r proceeds with (i) numbers U_v/D_e for the well depth and (ii) either Dunham r/r_0 (1) or Kratzer numbers r_0/r (3) or combinations like I (9). Fig. 12 shows that these scaling effects do not lead to a unification of the 5 PECs in the r/r_0-mode.

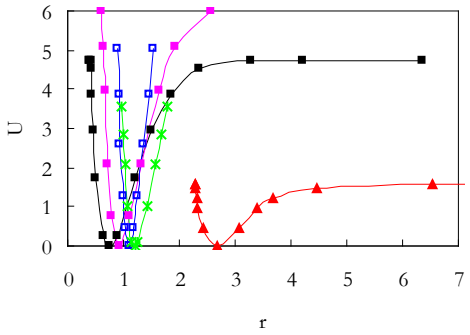

Fig. 11 RKR PECs for H_2 (black), HF(pink), I_2(red) N_2(blue) and O_2(green)

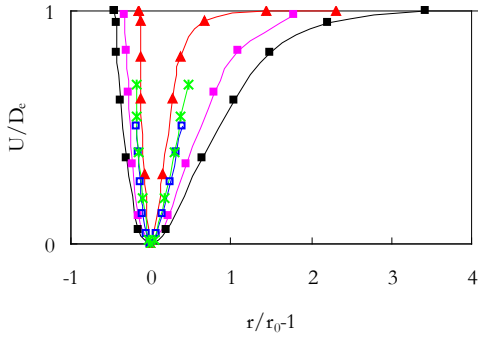

Fig. 12 Reduced PECs in r/r_0, centered at the origin (same colors)

For Kratzer representations in r_0/r, centered at the origin also, we choose I_s in Table 2-3. This gives Fig. 13. The asymmetry of PECs in Fig. 11 and 12 may be removed but, exactly as in Fig. 12, a single (universal) PEC is not yet obtained.

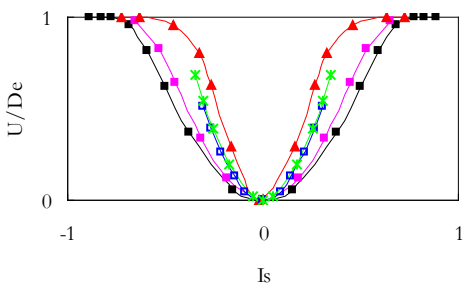

Fig. 13 Reduced PECs versus Kratzer-type I_s

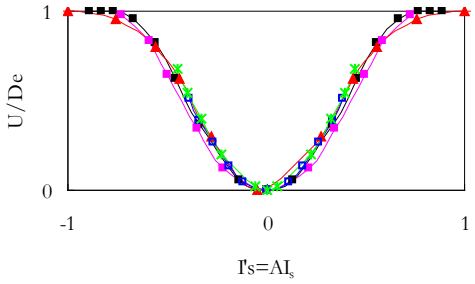

Fig. 14 Reduced PECs versus scaled I'_s

To make all PECs coincide, the essential role of a UPEF, an extra scale factor is needed for I_s, as U is properly normalized with D_e. Since the width of the well is determined by r_0 or by D_{ion}, as discussed above, this extra scale factor A should vary with r_0. We found (empirically) that

$$A=(r_0/r_{H2})^{1/4} \text{ and } I'_s=AI_s \qquad (25)$$

led to Fig. 14, which must be considered as a first attempt to produce a UPEC. Fig. 15 gives corresponding asymmetric PECs in $1/(1\pm AI_s)$-1, where PECs only nearly coincide. Unification is not yet perfect but the results strongly favor the existence of a UPEF. In reality, see Introduction, the genuine UPEC is already available by applying the results for H_2 above directly to all bonds. Plotting the 5 U_v/D_e sets versus $0{,}8x_q$ in (17)-(18) gives the genuine UPEC, shown in Fig. 16.

Unlike Fig. 15, Fig. 16 clearly shows that a single asymmetric PEC is generated for all 5 bonds with $1/(1\pm0{,}8x_q)$-1. The perfectly symmetric PEC of Mexican hat-type with $\pm0{,}8x_q$ is in Fig. 17. In Fig. 16, the full line is an aid to the eye, since a fit for these asymmetric PECs is impossible.

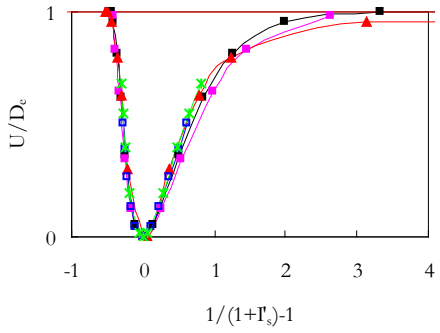

Fig. 15 Nearly coinciding PECs due to scaling by r_0

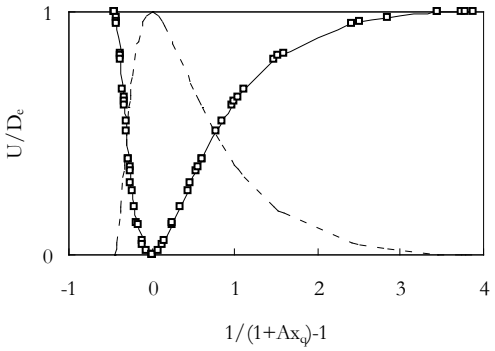

Fig. 16 Trivial, exact asymmetric UPEC (full), complementary UPEc (dashes)

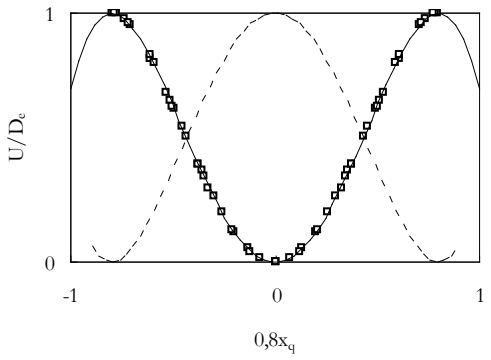

Fig. 17 Trivial symmetric UPEC of Mexican hat type (full line), complementary symmetric UPEC of Gauss type (dashes)

Fig. 16 also shows the complementary UPEC for $1-U_v/D_e$, which is, by definition, as asymmetric as the normal UPEC. The situation is different for the symmetric UPEC in Fig. 17. Here, the curve is an exact 4th order fit, given in Table 3. Extrapolated as in Fig. 8 for H_2, this symmetric UPEC is indeed a Mexican hat curve. The fit for the complementary $1-U_v/D_e$ (dashes) is equally exact, since trivial, but, in addition, this gives away a bell curve, typical for a normal Gauss distribution, which suggests that exponential fitting may be successful too (see further below). The covalent UPEC, based on a universal CHO, must not detract us from the fact that the Kratzer HO and corresponding Kratzer PEC for H_2 is fairly accurate, as shown in Section III (a). We cannot be complete, unless the trivial ionic UPEC of HO-type is also considered, for which numbers U/D_{ion} must be used, instead of U/D_e. These universal but trivial HO and CHO's are shown in Fig. X, both in r/r_0 and r_0/r version. First, we plot U_v/D_e versus x_q and U_v/D_{ion} versus d (12). For the 5 bonds, the ionic and covalent UPECs in the r_0/r-view are in Fig. 18.

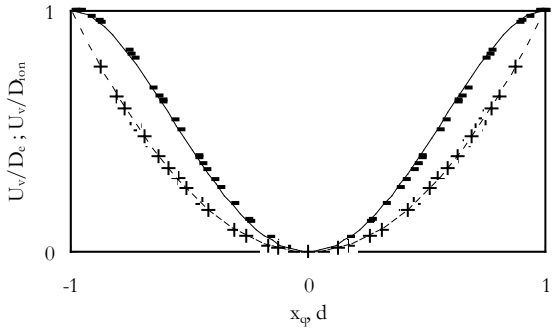

Fig. 18 U_v/D_e vs x_q (full -), U_v/D_{ion} vs d (dashes +):r_0/r-mode

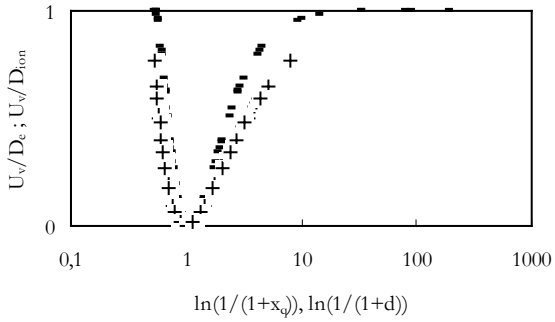

Fig. 19 Same as Fig. 18 but in r/r_0-mode

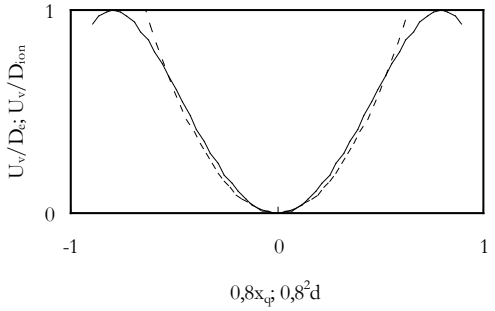

Fig. 20 U_v/D_e vs $0{,}8x_q$ (full), U_v/D_{ion} vs $0{,}8^2$d (dashes):r_0/r-mode

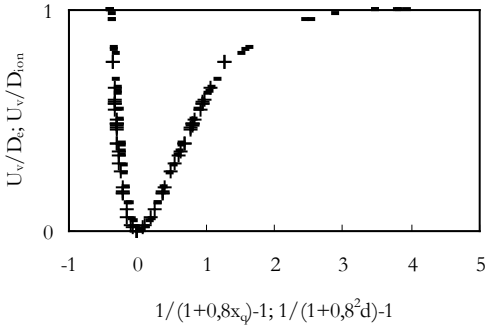

Fig. 21 Same as Fig. 20 but in r/r_0-mode

For the r/r_0-mode in Fig. 19, the largest r/r_0 value (H_2 level $0{,}99988D_e$) is $1/(1-0{,}994363)=177{,}4$. This enforces a logarithmic scale for the x-axis. Scaling by D_e leads to extremely large r-vales for the right branch, which are avoided with scaling by D_{ion}. Moderating x_q by factor 0,8, leads to $1/(1\pm0{,}8x_q)$, much more in line with RKR but it may be questioned whether or not this moderation is realistic. For the UPEC, this factor enlarges the 4th order term by $(5/4)^4=2{,}441$ (see Table 3). Adapting the ionic UPEC similarly, leads to the situation in Fig. 20-21, where the two PECs are much closer together and whereby very large r-values in Fig. 19 are avoided.
Fig. 20-21 illustrate how difficult it is to distinguish HO- from CHO-behavior. They equally illustrate how difficult it is to distinguish 19th century based ionic from modern (QM) covalent chemical bonding in the neighborhood of the minimum (see further below on ionic models). This leads us to a broader view on the role of D_{ion} as scaling aid for molecular constants.
(c) Comparing D_{ion} and D_e as scaling aids for 300 low order molecular constants
Since (25) suggests that the ultimate extra scaling factor to expose the reality of a UPEF depends on r_0 or $D_{ion}=½e_2/r_0$, we wished to verify this scaling hypothesis on a much larger scale. We compare scaling efficiencies of D_{ion} and D_e for over 300 bonds [7] using vibrational constant $\omega_e x_e$,

i.e. the coefficient Y_{20} for $(v+½)^2$ in the Dunham expansion[1]. The 314 bonds for which $\omega_e x_e$ was known in 1999 [7] are reviewed here without any prior selection: 95 bonds contain H, D or T with maximum $\omega_e x_e$=121,336 cm^{-1} for H_2 [27]; 219 other bonds have maximum 16,262 cm^{-1} for NO^+ [27]. For D_e and D_{ion}, scaling maxima are 90000 cm^{-1} (≈89462 cm^{-1} for CO [27]) and 80000 cm^{-1} (≈78321 cm^{-1} for H_2 [27]).

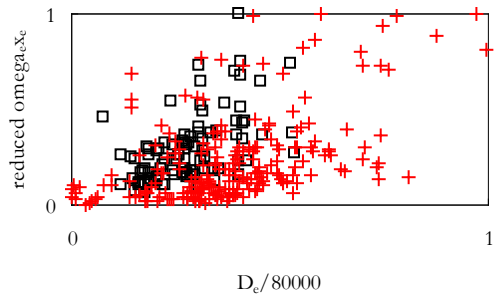

Fig. 22 Plot of reduced $\omega_e x_e$ vs reduced D_e (□ with H,D or T, + without)

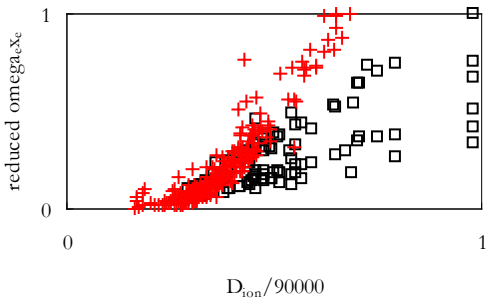

Fig. 23 Plot of reduced $\omega_e x_e$ vs reduced D_{ion} (□ with H,D,T, + without)

Fig. 22-23 reveal that, while there is almost no order in the plot with D_e, points are well ordered with D_{ion}. This confirms our conclusion above that scaling $\omega_e x_e$ will be more successful with D_{ion} than with D_e. Moreover, the spread of points for H,D,T-bonds in Fig. 23 closely follows a reduced mass classification: in the 6 classes for H, D, T (marks □), the upper series is for H-, the lower for T-containing bonds. This proves that for the spectroscopic constants, the scaling power of D_{ion} or r_0, as in (25), is greater that of D_e, as argued before [7].

More examples to illustrate this superior scaling power of D_{ion} for lower order constants (Dunham coefficients) are available [6-7,13-14] and must not be repeated here. Theoretically, this scaling power is now understood with the width (D_{ion} or r_0), not the depth of the well (D_e).

(d) Quantum information theory, Gauss probability density function for diatomic bonds

For 5 bonds, the universal Mexican hat curve and its complementary bell-curve are shown in Fig. 17. Table 2 shows that variable $(1/(1-I^2)$ will give a quartic PEC of type $(1/(1-I^2)-1)^2=I^4/(1-I^2)^2$ but, thus far, this functional was not yet detected.

However, we analyzed the bell-curve in Fig. 17, starting from the standard Gauss distribution of differences x from a mean value, given by

$$G(x)=e^{(-½x\hat{}2)}/\sqrt{(2\pi)} \qquad (26)$$

where mean μ is zero and standard deviation $\sigma^2=1$. To apply (26) for H_2 and the other bonds in Fig. X, we used PEC variable $(1/(1-I^2)-1)$ in Table 2 and reformed (26) in

$$(1-U_v/D_e)=G_I=e^{\{-A[1/(1-I\hat{}2)-1]\}} \qquad (27)$$

where A is a constant, related to r_0, and where $I=0,8x_q$, as above. With A=2,945, linear fit

$(1-U_v/D_e)= 1{,}00685e^{\{-2{,}945[1/(1-I\hat{}2)-1]\}}$ or $U_v \approx D_e(1-G_I)$ (28)

has a goodness of fit $R^2=0{,}99996$ and gives an average error for all 5 bonds of 140 cm^{-1}.

Although (27)-(28) give a phenomenological bonding approximation on the basis of a universal Gauss probability density function (PDF), (28) is more precise than any of the RKR PECs for H_2 (see Table 2). We remind that exponential fitting (28) always remains less accurate than fitting to order 4 in x_q, which is always exact due to (17), even for complementary $1-U_v/D_e$. This is evident from (18) and (20). Since $U_v/D_e=2x^2_q-x^4_q$ is, by virtue of (17), exact by definition, complementary $1-U_v/D_e=(1-x^2_q)^2$ is as exact. The curve can be approximated by a Gaussian like (26) but this is always accompanied with a loss of precision. These questions were already asked at the earlier stages of QM [15].

In practice and in terms of probabilities, intimately connected with wavefunctions in QM, (28) also confirms Kohn-Sham density functional theory models [28]. It shows the effect of Gauss type orbitals (GTO) and Slater type orbitals (STO) for the description of bonds, especially H_2. Extrapolating the quartic, obtained by plotting Gauss function (28) versus $0{,}8x_q$, reveals that also this curve has critical points at $\pm 0{,}8x_q$, as illustrated in Fig. 17.

In a less accurate bell curve approach, statistics and probabilities behind the universal PDF (UPDF) would result from a Bernoulli trial with a diatomic bond, confined to an infinitesimally thin coin. If heads were H_{AB}, referring to $H_A+H_B \rightarrow H_2$, tails are H_{BA}, referring to $H_B+H_A \rightarrow H_2$. At the top of the bell curve for H_2, uncertainty (certainty) about its origin is maximum (minimum). Only at the bottom of the bell curve, it is certain from which combination H_{AB} or H_{BA}, H_2 was formed. The H_2 coin is perfect, since H_{AB} and H_{BA} have equal probabilities for a homonuclear bond. However, a coin like model also implies that H_{AB} and H_{BA} exhibit chiral symmetry. This is easily understood, if the thin H_2 coin were a transparent sheet with marks + and – embedded. Tossing would result in marks in order +, - (heads) or in order -,+ (tails). Chiral symmetry for H_2 is in line with Hund [29], who showed that chiral symmetry is given away with a Mexican hat curve. Such curve was even detected in the Lyman series of atom H [30].

Nearly accurate probability/uncertainty approximations for H_2 may be explained by Heisenberg's principle [31] but they are obviously also connected with classical entropy (disorder) and with binary entropy as defined in information theory (Shannon [32], Fisher [33], R'enyi [34]).

(e) Theory of the chemical bond

A 5th application regards the 10-term QM Hamiltonian **H** for prototypical H_2. Using the standard notation for 4 charged particles: 2 leptons a, b and 2 nucleons A, B, we have

$U=½m_av^2_a+½m_bv^2_b+½m_Av^2_A+½m_Bv^2_B-e^2/r_{aA}-e^2/r_{bB}\pm(-e^2/r_{bA}-e^2/r_{aB}+e^2/r_{ab}+e^2/r_{AB})$ (29)

with 4 kinetic energy terms and 6 Coulomb potential energy terms. Reducing the 10 terms in

$$\mathbf{H}=½\Sigma(p^2_x/m_x)-e^2\Sigma(1/r_x) \quad (30)$$

is possible by symmetry considerations [17] but a classical alternative exists. The information on the uncertainties for the H_2 ground state, as described with a Gauss PDF and obeying a Bernoulli trial for coin-like H_2, derives from an ionic Kratzer HO or CHO model. The original 19th century ionic model is of electrostatic DC-type with anion and cation preserved, without dynamics but with a built in permanent electric dipole moment. The Gaussian view on H_2 learns that this ionic approach must be of AC-type, whereby it is uncertain which of the 2 bonding partners is the anion or the cation, wherein dynamics is involved and whereby the idea of a permanent electric dipole moment is no longer needed.. Still, ionic AC type bonding fully complies with the Kratzer bound state equation A(1)-A(2). For (29)-(30), this ionic AC model proves extremely useful. It leads to only one kinetic energy term instead of 4 and to only one Coulomb term instead of 6. For 2 atoms H, reduced mass is $\mu=m^2_H/(2m_H)=½m_H$. Two ions lead to a pseudo one-particle system with reduced mass

$$\mu_i=(m_H+m_e)(m_H-m_e)/(2m_H)=½m_H(1-m^2_e/m^2_H)=½m_H(1-2{,}963^{-7})\approx½m_H=\mu \quad (31)$$

Using levels U precise to order 0,001 eV, this small difference can safely be neglected.
With Coulomb attraction $-e^2/r$ between 2 ions in whatever order, we are left with only 2 terms

$$U_i=U_{ionic}(r)\approx½\mu_i v^2-e^2/r \text{ and } \mathbf{H}_i\approx½p^2_i/\mu_i-e^2/r \quad (32)$$

a considerable, if not drastic simplification over the 10 terms in (29) and (30) [13].
Next, for the equilibrium situation at r_0, we can use A(5) or

$$\mu_i v^2_0=e^2/r_0 \quad (33)$$

Plugging this in (32) returns

$$U_{i,0}=-½\mu_i v^2_0=-½e^2/r_0 \quad (34)$$

Since (32) is compatible with the original ionic Kratzer potential A(1)-A(2), U_i varies as

$$U_i=U_0(1-(1-r_0/r)^2=2r_0/r-(r_0/r)^2=2x-x^2 \quad (35)$$

formally identical to (15), the basis of the present analysis. Ionic bound state equation (35) is much simpler than (29)-(30), even for prototypical covalent bond H_2, and with the results for H_2 in Appendix 1, the ab initio character of this approach is well established.
Furthermore, (34)-(35) associate vibrations with the heavier particles, which is also the basis of the Franck-Condon recipe [35]. This led to Franck-Condon factors (FDFs), important for the interaction between ground and excited states. To expose more symmetry details, it may be useful to look at the vibrational spectra of excited states in a r_0/r mode too, rather than in a conventional r/r_0 mode,which may help to calculate precise FDFs [36].
The numerical bell curve for dimensionless H_2 as described by U_v/D_e, is easily associated with the exponential in the Morse potential and, more generally, with wavefunctions. Rather than giving

analytical details on these connections, however interesting, we compare our H_2 PEC directly with the H_2 PEC from ab initio QM.

(f) H_2 PEC by ab initio QM [37]

The H_2 PEC being so crucial for theory, it aroused the interest of theorists for nearly a century [37-43], starting with Heitler and London [43] in 1927. Ab initio QM calculations are tedious. Many parameters are needed and hundreds of wavefunctions are used [37]. Unfortunately, and as remarked in [11,23], none of the many QM PECs was ever published in analytical form: instead, U and r are tabulated. For the 1993 H_2 QM PEC, Wolniewicz [37] lists 54 r-values between 0,2 and $12r_B$, where r_B is the Bohr length, for which U is calculated. Points in this QM PEC are so close to the RKR PEC that a distinction between the 2 in a graph is impossible. As above (see also Table B1), we restrict the analysis to the 14 observed H_2 levels [22]. This leaves 33 points between $0,8r_B$ and $6r_B$. The absolutely exact, since trivial, PEC in x_q, as defined in our work by (17)-(18), i.e.

$$U_v=2D_ex^2_q-D_ex^4_q=-38292,984x^4_q+76585,968x^2_q \text{ cm}^{-1} \quad (36)$$

reproduces 33 U_v exactly. From r in [37], we calculated $r_0/r-1$ to find a link with x_q in (36). The difference between $0,8x_q$ in this work and $r_0/r-1$ from [37] is only 2,6 % for 33 levels. This is better than for the RKR PECs in Table 3. The QM H_2 PEC, graphically indistinguishable from the RKR H_2 PEC [5], and the PEC in this work are given in Fig. 24, where the Morse PEC is included for reference.

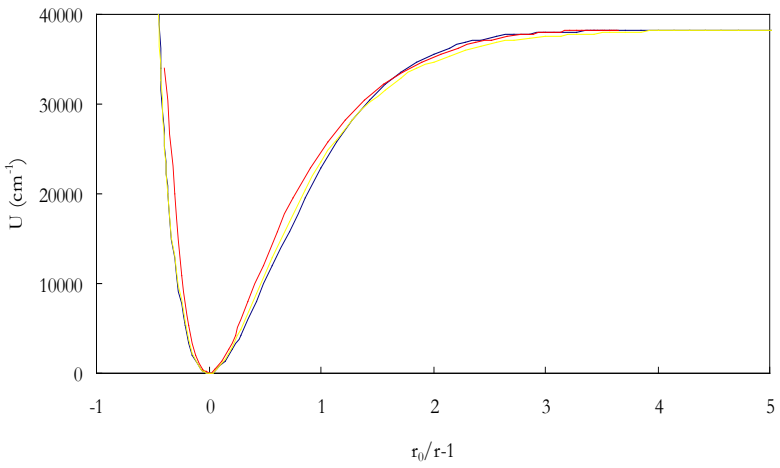

Fig. 24 Four H_2 PECs according to QM and RKR (black), this work (red) and Morse (yellow).

The general shape of the H_2 PEC is respected in all 4 schemes but discrepancies remain on curvatures between minimum and limit. However, of all 4 methods, only ours reproduces all U_v exactly with a simple analytical function (36), not provided by QM. In [37], U_v for $r=0,2r_B$ is greater than 700000 cm^{-1} or 18 times limit D_e. This contradicts the essence of this work, stating

that either branch of the H_2 PEC is limited to D_e and that the lower limit for r in the left branch is $½r_0$ (0,7r_B or 0,41 Å). With this extremely large U_v-value for r=0,2r_B, ab initio QM seems to have been inspired by the empirical Morse potential, which tolerates crossing of D_e at the repulsive branch, see Fig. 24. Similarly, the limit for the right branch is 7r_B or 3,7 Å, if A in Ax_q is constant and equal to 0,8=4/5. It remains to be verified whether or not this is acceptable.

Conclusion

A quartic Kratzer confined harmonic oscillator (CHO) for ground state H_2, itself hidden in the original Kratzer HO, implies that the theory of the chemical bond is much simpler than believed. This CHO gives rise to a H_2 PEC of Mexican hat-type. The long-standing problem about the universal molecular function (UPEF) is solved satisfactorily and analytically. Unlike QM, accurate PEFs and PECs are not only simple; they are analytically available. Entanglement of long- and short-range hydrogen quantum states is a classical, elementary arithmetic, physics element of RKR, itself a WKB approximation. Complementary PECs can be interpreted a Gaussian but only with loss of precision, which may be important for the EPR-paradox and related problems. Accepting these small discrepancies, quantum information theoretical concepts (entropy) seem to appear in a natural way. If so, H_2 would not only be prototypical for classical and modern physics and chemistry, for HO/CHO and for braid theory but even for quantum information theory.
At the Bohr scale, a Kratzer-Coulomb law smoothly accounts for minimum and extremes at either side of this minimum for bond H_2, the prototypical 4 unit-charge system with 4 charges pair-wise conjugated. Since we dealt successfully with 2-nucleon system H_2 in the context of a RKR-WKB model, a similar Kratzer scheme may be useful at the nuclear scale [20], where nucleon interactions are the rule.

References

[1] M. Moshinsky and Y.F. Smirnov, *The harmonic oscillator in modern physics*, Taylor & Francis, 1996, 414 p.
[2] L. Pauling and E.B. Wilson, *Introduction to Quantum Mechanics with applications to chemistry*, McGraw-Hill, New York, 1935, 468 p.
[3] a R. Rydberg, Z. Physik **73**, 376 (1931); b O. Klein, Z. Physik **76**, 221 (132); c A.L.G. Rees, Proc. Phys. Soc. (London) **59**, 998 (1947)
[4] W.M. Kosman and J. Hinze, J. Mol. Spectrosc. **56**, 93 (1975); C.R. Vidal and H. Scheingraber, J. Mol. Spectrosc. **65**, 46 (1977)
[5] D. Steele, E.R. Lippincott and J.T. Vanderslice, Rev. Mod. Phys. **34** 239 (1962)
[6] G. Van Hooydonk, Z. Naturforsch. **A 37** 710 (1982)
[7] G. Van Hooydonk, Eur. J. Inorg. Chem., Oct. 1617 (1999)
[8] Y.P. Varshni, Rev. Mod. Phys. **29** 664 (1957); ibid. **31** 839 (1959)
[9] Y.P. Varshni, Chem. Phys. **342** 297 (2007); idid. **353** 32 (2008)
[10] J.L. Graves and R.G. Parr, Phys. Rev. A **31** 1 (1985)
[11] J. Tellinghuisen, S.D. Henderson, D. Austin, K.P. Lawley and R.J. Donovan, Phys. Rev. A **39** 925 (1989)

[12] A. Kratzer, Z. Phys. **3** 289 (1920); Ann. Phys. **67** 127 (1922); E. Fues, Ann. Phys. **80** 376 (1926)
[13] G. Van Hooydonk, Z. Naturforsch. A **64** 810 (2009)
[14] G. Van Hooydonk, Phys. Rev. Lett. **100** 159301 (2008)
[15] A. Einstein, B. Podolsky and N. Rosen, Phys. Rev. **47**, 777 (1935); J.S. Bell, Rev. Mod. Phys. **38** 447 (1966)
[16] M. A. Nielsen and I. Chuang, Am. J. Phys. **70**, 558 (2002); V. Vedral, Rev. Mod. Phys. 74, 197 (2002); F. Benatti, *Quantum information Theory*, in Theoretical and Mathematical Physics, Springer,, 2009
[17] G. Van Hooydonk, Eur. Phys. J. D **32** 299 (2005)
[18] J.L. Dunham, Phys. Rev. **41** 713 (1932)
[19] G. Simons and J.M. Finlan, Phys. Rev. Lett. **33**, 131 (1974)
[20] L. Fortunato, Eur. Phys. J. A **26**, s01, 1 (2005)
[21] P.M. Morse, Phys. Rev. **34**, 57 (1929)
[22] I. Dabrowski, Can. J. Phys. **62** 1639 (1984)
[23] G. Van Hooydonk and Y.P. Varshni, arxiv:0906.2905
[24] D.R. Herschbach, RKR method at http://faculty.physics.tamu.edu/herschbach
[25] F. Wilczek, Physics **4**, 10 (2011)
[26] P. Bonderson, V. Gurarie and C. Nayak, Phys. Rev. B **83**, 075303 (2011)
[27] K.P. Huber and G. Herzberg, *Molecular Spectra, Molecular Structure: Constants of Diatomic Molecules*, vol. IV, Van Nostrand-Reinhold, New York, 1979
[28] W. Kohn and L.J. Sham, Phys. Rev. 140 1133 (1965); R.G. Parr and W. Yang, *Density-Functional Theory of Atoms and Molecules,* Oxford University Press, 1994
[29] F. Hund, Z. Phys. **43** 805 (1927)
[30] G. Van Hooydonk, Acta Phys. Hung. A NS **19**, 385 (2004)
[31] W. Heisenberg, Z. Phys. **43** 172 (1927)
[32] C.E. Shannon, Bell Syst. Tech. **27** 379 (1948); ibid. **27** 623 (1948)
[33] R.A. Fisher, Proc. Cambridge Phil. Soc. **22** 700 (1925)
[34] A. R´enyi, Proc. Fourth Berkeley Symposium on Mathematics, Statistics and Probability, Berkeley University Press, 1960; Probability Theory, Amsterdam, North-Holland, 1960
[35] J. Franck, Trans. Farad. Soc. **21** 536 (1926); E. Condon, Phys. Rev. **28** 1182 (1926)
[36] M. Toutounji, J. Chem. Phys. **128** 164103 (2008)
[37] L. Wolniewicz, J. Chem. Phys., **103** 1792 (1995) and references therein
[38] W. Kolos and C.C.J. Roothaan, Rev. Mod. Phys. 32, 219 (1960).
[39] W. Kolos and L. Wolniewicz, J. Chem. Phys. **49** 404 (1968)
[40] W. Kolos and L. Wolniewicz, J. Mol. Spect. **54** 303 (1975)
[41] D. Kedziera et al., J. Chem. Phys. **125** (2006)
[42] K. Pachucki and J. Komasa (2008), arxiv:0811.4355v2
[43] W. Heitler and F. London, Z. Phys. **44** 455 (1927)
[44] P.J. Mohr and B.N. Taylor, Rev. Mod. Phys. **77**, 1 (2005); http://physics.nist.gov/constants

Appendix A. Kratzer predictions for bond H_2 [13]

Conceptually, the original *ionic* Kratzer potential [12]

$$U_K=-e^2/r+B/r^2 \qquad A(1)$$

behind (4) in the text has advantages [13]. First, searching for a minimum with dU/dr=0 provides with $B=½e^2r_0$ and gives

$$U_K=-e^2/r+½e^2r_0/r^2=½(e^2/r_0)[2r_0/r-(r_0/r)^2]=D_{ion}(2x-x2)=U_0(2x-x^2) \qquad A(2)$$

Secondly, searching for the force constant with $d^2U/d^2r=k_e$ leads to

$$k_e=e^2/r^3_0 \qquad A(3)$$

This analytical result for k_e is impossible with Dunham's potential, which needs observed U-data to get k_e. Dunham's procedure $½k_er^2_0=a_0$ can now be completed with $½k_er^2_0=a_0=D_{ion}=½e^2/r_0$. As a result, H_2 fundamental frequency ω is obtained directly from A(3) since

$$2\pi\omega=\sqrt{(k_e/\mu)}=\sqrt{[2e^2/(m_Hr^3_0]} \qquad A(4)$$

This equilibrium result can also be written as

$$\mu v^2_0=e^2/r_0 \qquad A(5)$$

Finally, if r_0 were available from mass m_H, the complete Kratzer H_2 HO and parabolic PEC are available without any other assumption [13]. To reach a full *ab initio* solution for this HO, the classical 19th century relation between mass, density γ and radius of sphere-like H [13] gives

$$m_H=(4\pi\gamma/3)r^3_0 \qquad A(6)$$

Assuming only m_H is known (m_H=1837,15267247m_e [44]) and that γ=1, A(6) leads to

$$r_0=0{,}736515 \text{ Å} \qquad A(7)$$

Table A1 shows all H_2 spectroscopic characteristics derived from Kratzer potential A(1).

Table A1 H_2 constants from Kratzer potential and the H_2 spectrum [22,27] (m_H=1,67353.10^{-24} g [44])

	Kratzer result	from the spectrum [18]	% diff
($\mu=½m_H$	8,367663.10^{-25} g	also assumed known)	
r_0	0,73652 Å	0,74144 Å	-0,66
ω	4410,173 cm^{-1}	4401,213 cm^{-1}	0,20
k_e	577452,8805 force/cm	575108,9041 force/cm	0,41
$a_0=D_{ion}$	78844,9005 cm^{-1}	79578,4482 cm^{-1}	-0,92
D_0 (a)	36110,245 cm^{-1}	36118,344 cm^{-1}	-0,02
D_e (a)	38281,14 cm^{-1}	38292,984 cm^{-1}	-0,02

(a) from a recent analysis of the H_2 spectrum with a Kratzer variable [23]

The Kratzer H_2 HO or the parabolic PEC is completely known with m_H [44] and D_{ion}, k_e and ω directly available from the above equations.

Appendix B Comparing observed H_2 levels [22] with RKR levels [5]

Although we adhered to H_2 level data as given in [5] for reasons of transparency, more precise data are available [22]. In Table B1, columns 1-3 give H_2 data for v, ΔG_v and U_v as observed by Dabrowski [20]. Columns 4-5 give v+½, not in [5], and levels, adapted for zero point energy ½ω. Columns 6 contains levels in [5], converted with 1eV=8065,479 cm^{-1}. To verify the consistency of levels in [5], we calculated ZPE by taking the difference U_v [22]-$U_{v+½b}$[5] in column 6. This shows that, with the levels in [5], ZPE varies between 2166 and 2171 cm^{-1}, in line with an expected uncertainty of 8 cm^{-1} for data, given to order 0,001 eV. These discrepancies are too small to have an effect on the theory as applied in this work. However, the levels in the 2 lower rows for long-range behavior of H_2 are clearly not observed in [22]. They are not repeated at small r in the original paper either [5], as already indicated in Table 1.

Table B1 Observed H_2 levels [22], RKR levels [5] and zero point energies ZPE

v	ΔG_v [22]	U_v [22]	v+½	$U_{v+½}$[a]	$U_{v+½}$[5]	ZPE=$U_{v+½b}$[5]-U_v[22]
0	(4401,21_3)	0	0,5	2170,85	2170	2171
1	4161,14	4161,14	1,5	6331,99		
2	3925,79	8086,93	2,5	10257,78		
3	3695,43	11782,36	3,5	13953,21	13953	2171
4	3467,95	15250,31	4,5	17421,16		
5	3241,61	18491,92	5,5	20662,77		
6	3013,86	21505,78	6,5	23676,63	23672	2166
7	2782,13	24287,91	7,5	26458,76		
8	2543,25	26831,16	8,5	29002,01		
9	2292,93	29124,09	9,5	31294,94	31294	2170
10	2026,38	31150,47	10,5	33321,32		
11	1736,66	32887,13	11,5	35057,98		
12	1415,07	34302,20	12,5	36473,05	36472	2170
13	1049,16	35351,36	13,5	37522,21		
14	622,02	35973,38	14,5	38144,23	38142	2169
?			level not measured		38271[b]	
?			level not measured		38287[b]	

[a] zpe (zero-point energy) 2170,849 cm^{-1} [23]

[b] Given ΔG_v for v=14 in Column 2, the last observed level is more than 600 cm^{-1} below the dissociation limit. This implies that these 2 levels in [5] are not observed. These levels and their turning points, critical for long range H_2 behavior, may well have been inspired by the Morse-potential [21]. This also justifies the limit of 33, set to the 55 data points for the QM H2 PEC [37] (see text).